

Study on secondary electron suppression in compact D–D neutron generator

Zhi-Wu Huang¹ · Xiao-Hou Bai¹ · Chang-Qi Liu¹ · Jun-Run Wang^{1,2} · Zhan-Wen Ma¹ · Xiao-Long Lu^{1,2} · Zheng Wei^{1,2} · Zi-Min Zhang³ · Yu Zhang¹ · Ze-En Yao^{1,2}

Received: 12 September 2018 / Revised: 4 November 2018 / Accepted: 9 November 2018 / Published online: 26 April 2019
© China Science Publishing & Media Ltd. (Science Press), Shanghai Institute of Applied Physics, the Chinese Academy of Sciences, Chinese Nuclear Society and Springer Nature Singapore Pte Ltd. 2019

Abstract A compact D–D neutron generator, with a peak neutron yield of D–D reactions up to 2.48×10^8 n/s is being developed at Lanzhou University in China for application in real-time neutron activation analysis. During tests, the problem of back acceleration of secondary electrons liberated from the neutron production target by deuterium ions bombardment was encountered. In this study, an electric field method and a magnetic field method for suppressing secondary electrons are designed and experimentally investigated. The experimental results show that the electric field method is superior to the magnetic field method. Effective suppression of the secondary electrons can be achieved via electrostatic suppression when the bias voltage between the target and the extraction-accelerating electrode is > 204 V. Furthermore, the secondary electron emission coefficient for the mixed deuterium ion (D_1^+ , D_2^+ , and D_3^+) impacting on molybdenum is estimated. In

the deuterium energy range of 80–120 keV, the estimated secondary electron emission coefficients are approximately 5–5.5 for the mixed deuterium ion glancing incidence of 45° and approximately 3.5–3.9 for the mixed deuterium ion normal incidence.

Keywords D–D neutron generator · Secondary electron suppression · Secondary electron emission coefficient

1 Introduction

Compact neutron generators based on $^2\text{H}(d,n)^3\text{He}$ (D–D) and $^3\text{H}(d,n)^4\text{He}$ (D–T) fusion reactions are among the most important neutron sources. With advantages over isotropic neutron sources in the radiation safety and the neutron output adjustability, they have important applications in scientific research and neutron application technologies, such as neutron imaging [1] and neutron activation analysis [2–4]. A compact D–D neutron generator (CDDNG) with a peak neutron output of up to 2.48×10^8 n/s is being developed at Lanzhou University for real-time neutron activation analysis [5].

The scheme of the CDDNG is shown in Fig. 1. The outline of the CDDNG is a cylinder with a length of 984 mm and a diameter of 234 mm. The CDDNG consists of an ion source, an extraction-accelerating electrode, a target assembly, a high-voltage insulator assembly, a vacuum vessel, and a vacuum system. Deuterium ions are produced from a duoplasmatron ion source. To simplify the mode of power supply and ensure the safety and reliability during operation, a negative high voltage is applied to the target, and the ion source is kept at ground potential. The gap between the extraction-accelerating electrode and the

This work was supported by the National Key Scientific Instrument and Equipment Development Project of China (2013YQ40861), the National Natural Science Foundations of China (11875155, 11705071), and the Fundamental Research Funds for the Central Universities of China (lzujbky-2019-kb09).

✉ Yu Zhang
zhyu@lzu.edu.cn

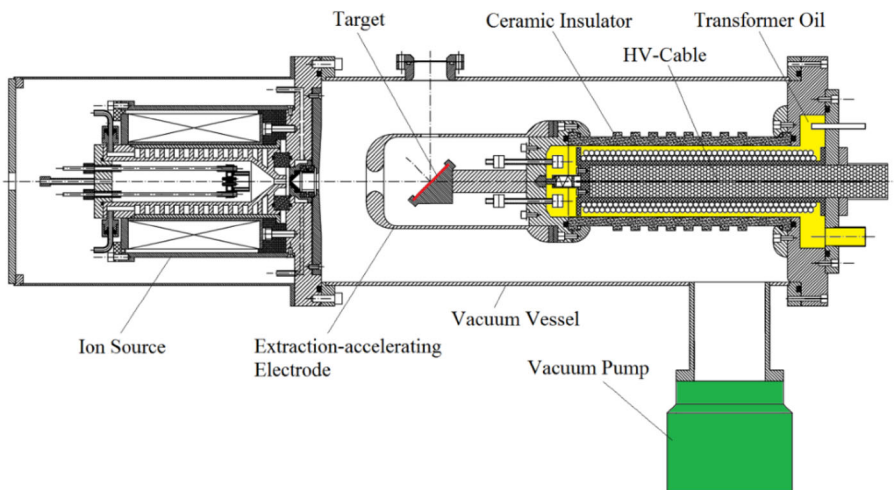
✉ Ze-En Yao
zeyao@lzu.edu.cn

¹ School of Nuclear Science and Technology, Lanzhou University, Lanzhou 730000, China

² Engineering Research Center for Neutron Application Technology, Ministry of Education, Lanzhou University, Lanzhou 730000, China

³ Institute of Modern Physics, Chinese Academy of Sciences, Lanzhou 730000, China

Fig. 1 Scheme of the compact D–D neutron generator



plasma electrode of the ion source is 55 mm. Negative high voltage is applied to the extraction-accelerating electrode with the aid of the high-voltage insulator assembly and a high-voltage cable. The electric field is generated between the ion source and the extraction-accelerating electrode to extract and accelerate the deuterium ions to the target where neutrons are produced by D–D nuclear reactions. To achieve a longer target lifetime, a self-loading solid molybdenum target (50 mm in diameter and 1 mm in thickness) is used as the neutron production target. The surface of the target is 45° to the beam direction. A high vacuum degree ($\sim 10^{-4}$ Pa) in the vacuum vessel is provided by a set of vacuum pump systems, which consist of a mechanical pump and a turbo molecular pump. The target is cooled by fluorine-containing coolant (3 M Fluorinert FC-3283), which is pumped to the back of the target through the pipe. To achieve an excellent high-voltage insulation performance, the ceramic insulator tube is filled with transformer oil.

Because the extraction-accelerating electrode and the target are at negative potential and the ion source is at ground potential, secondary electrons released from the target surface which bombarded with deuterium ions [6] will be accelerated back to the ion source, producing a secondary electron current. This effect will increase the load of the high-voltage power supply [7] and will produce frequent high-voltage breakdown [8] and significant bremsstrahlung X-ray emission [9, 10]. These effects affect both the accurate measurement of the deuterium ion current on the target [11, 12] and the stable operation of the CDDNG [8], as well as posing a potential radiation safety hazard [9]. Therefore, it is imperative to find a suitable way to suppress the secondary electrons.

In this study, an electric field method and a magnetic field method [13–15] for suppressing the secondary electrons are designed and experimentally investigated. In

addition, the secondary electron emission coefficient for deuterium ion impacting on molybdenum is estimated.

2 Experimental methods and results

2.1 Electric field method

The scheme of the designed electric field method for suppressing the secondary electrons is shown in Fig. 2. A ceramic ring is used to isolate the target from the extraction-accelerating electrode. A resistor (R) is used to connect the extraction-accelerating electrode to the target. When the deuterium current bombards the target and flows through the resistor to the extraction-accelerating electrode, a bias voltage is generated between the target and the extraction-accelerating electrode. The bias voltage (V_b) of the target relative to the extraction-accelerating electrode can be estimated with the following equation

$$V_b = I_d \cdot R \tag{1}$$

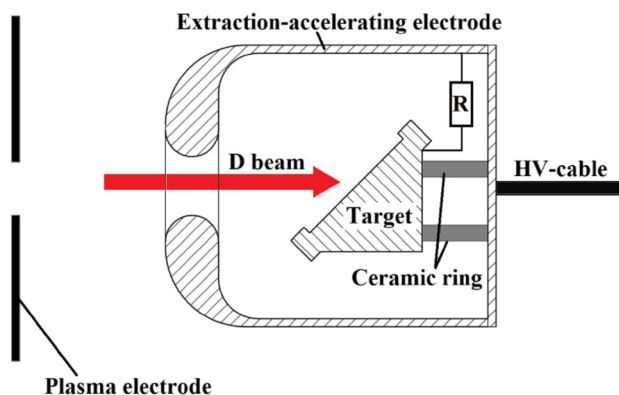


Fig. 2 Scheme of the electrostatic suppression

where I_d is the deuterium ion current on the target. A current of secondary electrons, which is formed by the secondary electrons hitting the extraction-accelerating electrode, also affects the calculation of V_b through the resistor R to the target. The aim of this experiment is to obtain the threshold suppression voltage at which the secondary electrons are effectively suppressed. In this case, the secondary electron current can be negligible.

According to Eq. (1), when I_d is constant, V_b increases linearly with increasing R . The secondary electrons should be completely suppressed when V_b is large enough. To study the performance of the secondary electron suppression of the electric field method shown in Fig. 2, experimental measurements of the high-voltage load current (I_{load}) with the accelerating voltage (V_{ex}) are taken under the same arc current (I_{arc}) of the ion source and various resistors ($R = 0\text{ k}\Omega$, $R = 10.2\text{ k}\Omega$, $R = 51.1\text{ k}\Omega$, $R = 102\text{ k}\Omega$, $R = 133.2\text{ k}\Omega$, $R = 200\text{ k}\Omega$, $R = 400\text{ k}\Omega$, and $R = 500\text{ k}\Omega$). The high-voltage load current I_{load} is the read back of the high-voltage power supply to the given high voltage. These resistance values are obtained by a combination of different metal film resistors. The rated power of a single metal film resistor is 2 W. The current I_{load} should be the sum of the extraction deuterium current (I_d), the secondary electron current (I_e), and the leakage current of high voltage (I_{leak}):

$$I_{load} = I_d + I_e + I_{leak} \tag{2}$$

The experimental results of I_{leak} , with $I_d = 0\text{ mA}$, show that I_{leak} will not be $> 0.1\text{ mA}$ even at accelerating voltage of 150 kV; thus, I_{leak} can be ignored. Therefore, I_{load} can be approximately calculated as the sum of I_d and I_e :

$$I_{load} \approx I_d + I_e \tag{3}$$

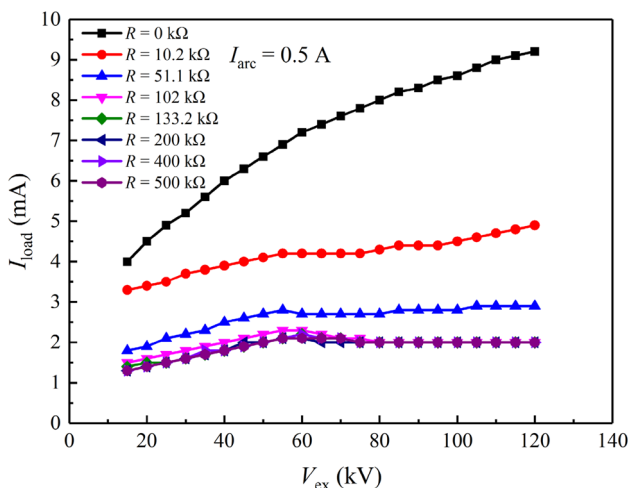


Fig. 3 The load current (I_{load}) as a function of the accelerating voltage (V_{ex}) for different resistances (R), with $I_{arc} = 0.5\text{ A}$

Figure 3 shows the experimental results of I_{load} as a function of the accelerating voltage (V_{ex}) for various resistances (R) under the same arc current (I_{arc}) of the ion source. As shown in Fig. 3, for $R = 0\text{ k}\Omega$ ($V_b = 0\text{ V}$), I_{load} increases rapidly with increasing V_{ex} and when $V_{ex} = 120\text{ kV}$, I_{load} is up to 9.2 mA. As R increases, the increase in I_{load} becomes slower with increasing V_{ex} and at the same V_{ex} , I_{load} decreases rapidly. This means that more and more secondary electrons are suppressed and when $R = 0\text{ k}\Omega$ ($V_b = 0\text{ V}$), a large part of I_e is in part of the I_{load} . When $R \geq 102\text{ k}\Omega$ and $V_{ex} \geq 80\text{ kV}$, I_{load} becomes a constant of 2 mA. This suggests that the secondary electrons have been completely suppressed, and I_{load} is equal to I_d . In other words, the effective secondary electrons suppression can be achieved when the bias voltage between the target and the extraction-accelerating electrode is greater than or equal to 204 V [the product of $R = 102\text{ k}\Omega$ and $I_d = 2\text{ mA}$ from Eq. (1)].

2.2 Magnetic field method

The designed magnetic field method for suppressing secondary electrons is shown in Fig. 4a. A pair of magnets is aligned with opposite poles facing each other to produce a magnetic field parallel to the target surface. The target is connected to the extraction-accelerating electrode through a wire. The $\text{Sm}_2\text{Co}_{17}$ permanent magnet is selected because of its high remanent flux density and thermostability. Under three different permanent magnet sizes ($\Phi 20\text{ mm}$ (diameter) $\times 5\text{ mm}$ (thickness), $\Phi 20\text{ mm}$ (diameter) $\times 10\text{ mm}$ (thickness), and $\Phi 20\text{ mm}$ (diameter) $\times 12\text{ mm}$ (thickness)), the magnetic field distributions along the center axis of the magnets (the red line in Fig. 4a) are measured with a Hall magnetometer. The results are shown in Fig. 4b. The magnetic field strength at the center of the target surface ($X = 0\text{ mm}$) is approximately 76 Gauss for $\Phi 20\text{ mm}$ (diameter) $\times 5\text{ mm}$ (thickness), 131 Gauss for $\Phi 20\text{ mm}$ (diameter) $\times 10\text{ mm}$ (thickness), and 150 Gauss for $\Phi 20\text{ mm}$ (diameter) $\times 12\text{ mm}$ (thickness).

To study the performance of secondary electron suppression of the magnetic field method shown in Fig. 4a, the load current (I_{load}) as a function of the accelerating voltage (V_{ex}) was measured with and without a magnet (three different sizes) under the same arc current (I_{arc}) of the ion source. The experimental results are shown in Fig. 5. It can be seen that I_{load} is significantly lower with the $\text{Sm}_2\text{Co}_{17}$ magnets. The secondary electrons can be suppressed by the designed magnetic field method. When the magnet size is $\Phi 20\text{ mm}$ (diameter) $\times 5\text{ mm}$ (thickness), the secondary electrons are not completely suppressed. The effects of secondary electron suppression with the magnets of size $\Phi 20\text{ mm}$ (diameter) $\times 10\text{ mm}$ (thickness) and $\Phi 20\text{ mm}$

Fig. 4 Placement of the permanent magnets (a); magnetic field distributions along the center axis of the magnets for different magnet sizes (b)

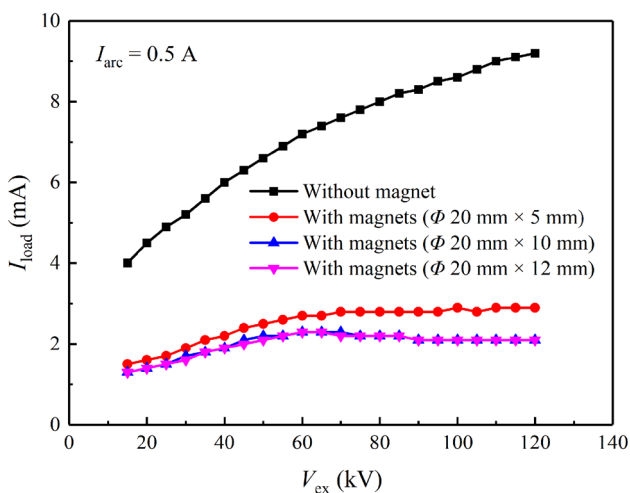
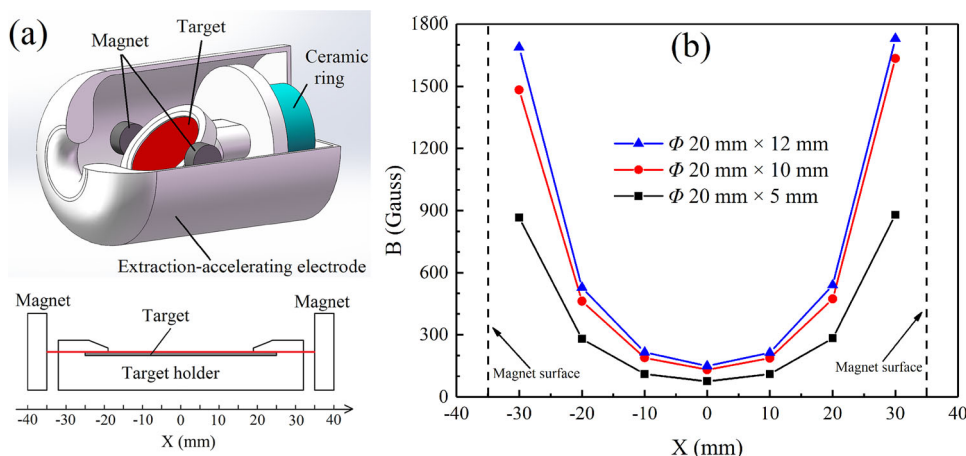


Fig. 5 Load current (I_{load}) as a function of accelerating voltage (V_{ex}) with and without magnets, with $I_{arc} = 0.5$ A

(diameter) \times 12 mm (thickness) are superior than those with the Φ 20 mm (diameter) \times 5 mm (thickness) magnets.

2.3 Comparison of the electrostatic and magnetic suppressions

Both the electric field and magnetic field methods affected the suppression of secondary electrons. To compare their performance in secondary electrons suppression, the dependence of I_{load} on V_{ex} for different arc currents (I_{arc}) of the ion source was measured with the electric field method with $R = 500$ k Ω and the magnetic field method with the magnet of size Φ 20 mm (diameter) \times 12 mm (thickness). During the experiment, the accelerating voltage (V_{ex}) was increased over time from 15 kV to 120 kV, in steps of 5 kV, and the arc current (I_{arc}) was increased over time from 0.4 A to 0.8 A, in steps of 0.2 A. The experimental results are shown in Fig. 6. As shown

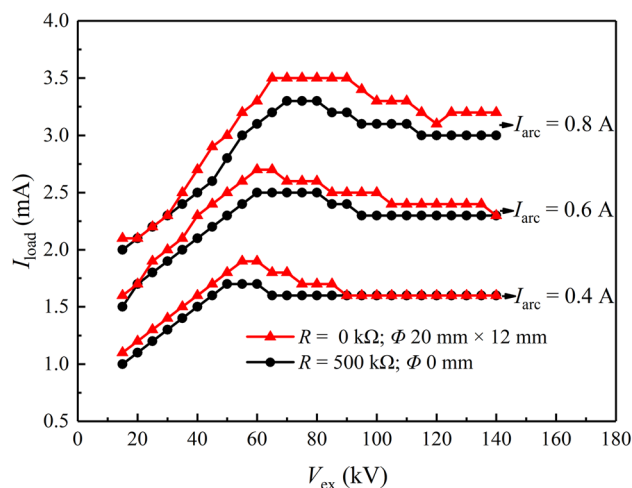


Fig. 6 Load current (I_{load}) as a function of the accelerating voltage (V_{ex}) with different I_{arc} for electrostatic suppression with $R = 500$ k Ω and magnetic suppression with the magnet of size Φ 20 mm (diameter) \times 12 mm (thickness)

in the figure, for different I_{arc} , the I_{load} gradually reaches a stable value with increasing V_{ex} in both methods. This confirms that both methods can effectively suppress secondary electrons. However, the I_{load} with the magnetic field method is significantly higher than that with the electric field method, while the I_{arc} of the ion source is higher in the former. A higher arc current (I_{arc}) means a bigger deuterium ion beam, that is, the suppression effect of the magnetic field will become worse as the deuterium ion beam increases. There are two possible reasons for this: One is the space charge effect, which can occur in the vicinity of the target, and the other is the demagnetization of the permanent magnet due to ion bombardment and heat conduction from the target.

In summary, the designed electric field method is superior to the magnetic field method for secondary electrons suppression. Therefore, the electric field method will be employed in our CDDNG. For a better suppression

effect in a lower deuterium ion current, the resistance should be 500 k Ω . The resistance is located in the transformer oil of the high-voltage insulator assembly to achieve good cooling. After the implementation of the designed electric field method, the CDDNG was continuously operated for more than 3 h without high-voltage breakdown. When measures to suppress secondary electrons are not taken, high-voltage breakdown occurs frequently, especially when the load current is close to 10 mA. Furthermore, the dose of X rays is reduced by about 10 times.

2.4 Estimation of the secondary electron emission coefficient

In this section, the secondary electron emission coefficient for deuterium ions incident on molybdenum is estimated based on the experimental data of the electrostatic suppression shown in Fig. 3. The secondary electron emission coefficient should be the ratio of the number of secondary electrons ejected from the target to the number of incident deuterium ions. It is assumed that the secondary electrons are not suppressed at all with $R = 0$ k Ω , and are completely suppressed with $R = 500$ k Ω and $V_{\text{ex}} > 80$ kV. According to the experimental data in Fig. 3, the secondary electron emission coefficient λ of deuterium beam incident on molybdenum can be estimated by the following equation:

$$\lambda(E_d) = \frac{I_{\text{load}(0,E_d)} - I_{\text{load}(500,E_d)}}{I_{\text{load}(500,E_d)}}, \quad (4)$$

where E_d , which is approximately equal to the product of V_{ex} and the charge of deuterium ion, is the energy of the deuterium ion, $I_{\text{load}(0,E_d)}$ is the high-voltage load current for $R = 0$ k Ω , and $I_{\text{load}(500,E_d)}$ is the high-voltage load current for $R = 500$ k Ω .

However, some secondary electrons can be suppressed even if $V_b = 0$ V (i.e., $R = 0$ k Ω), owing to the target being installed inside the cavity of the cylindrical extraction-accelerating electrode (see Fig. 2). In other words, $I_{\text{load}(0,E_d)} - I_{\text{load}(500,E_d)}$, which does not include the suppressed secondary electron current, is only the back-accelerated secondary electron current for $R = 0$ k Ω . If the coefficient λ is directly estimated according to the experimental data in Fig. 3 and Eq. (4), it will be underestimated. If the ratio (η) of the back-accelerated secondary electrons to the total secondary electrons ejected from the target can be found, Eq. (4) can be modified to:

$$\lambda(E_d) = \frac{I_{\text{load}(0,E_d)} - I_{\text{load}(500,E_d)}}{I_{\text{load}(500,E_d)}} \cdot \frac{1}{\eta} \quad (5)$$

It is quite difficult to measure the value of η . Therefore, a simulation investigation on the transport of the secondary

electrons was carried out by a PIC code [16]. In the simulation, we skip the complex physical process of the secondary electrons produced by the deuterium ion interaction with the target [17], because electrons are produced as long as the deuterium ions are incident on the target surface. It is assumed that a deuterium ion produces three secondary electrons. The angular distribution of electrons ejected is set to be a cosine distribution. After contact with the target, the deuterium ions are ‘killed,’ which means they disappear in the subsequent simulation, irrespective of the cascade effect of the secondary electrons, which means that the secondary electrons disappear directly after hitting any electrode and there is no secondary particle production. The current of deuterium ions is 2 mA.

A typical simulation image of the space distribution of the secondary electrons is shown in Fig. 7a, under $V_{\text{ex}} = 120$ kV and $R = 0$ k Ω . Figure 7b shows the potential distribution between the extraction-accelerating electrode and the target. The value of η can be calculated by counting the number of secondary electrons on each electrode. The calculated results of η are shown in Fig. 7c, with V_{ex} increasing from 80 to 120 kV in steps of 10 kV. The value of η as a function of V_{ex} shows a good linear relationship. The linear fitting values of η are used to calculate the coefficient λ . Figure 8 shows the calculated results of the coefficient λ according to Eq. (5) with the correction of the ratio η . It can be seen that λ increases with increasing deuterium beam energy. In the energy range of 80–120 keV, the value of λ is between 5 and 5.5 with a deuterium ion glancing incidence of 45°.

The secondary electron emission coefficient on the metal target bombarded by deuterium ion has been widely investigated in the past decades [18–20]. However, most of these studies were carried out under the condition of normal incidence. According to references [21, 22], the secondary electron emission coefficient with glancing incidence of 45° (λ_{45°) can be calculated by the following equation

$$\lambda_{45^\circ} = \lambda_{\perp} \cdot \cos^{-1}(45^\circ), \quad (6)$$

where λ_{\perp} is the secondary electron emission coefficient under normal incidence. For comparison with the previous data, we convert λ_{45° into λ_{\perp} according to Eq. (6). Figure 8 shows the calculated results. The value of coefficient λ_{\perp} is between 3.5 and 3.9 at energies of 80–120 keV. The experimental data from Ref. [20] for the deuterium ions (D_1^+) normally incident on molybdenum are also shown in Fig. 8. It can be seen that λ_{45° is bigger than λ_{\perp} . This is because the glancing incidence leads to a shallower penetration and it makes it easier for the generated carriers to exit the target surface. Furthermore, our estimated results (λ_{\perp}) are significantly greater than the experimental data from Ref. [17]. The reason is that the mixed deuterium ion

Fig. 7 **a** Space distribution of the secondary electrons for $V_{ex} = 120$ kV and $R = 0$ k Ω ; **b** potential distribution between the extraction-accelerating electrode and the target, where T and E denote the target and the extraction-accelerating electrode, respectively; **c** ratio of the back-accelerated secondary electrons to the total secondary electrons (η) ejected from the target as a function of V_{ex} , for $R = 0$ k Ω

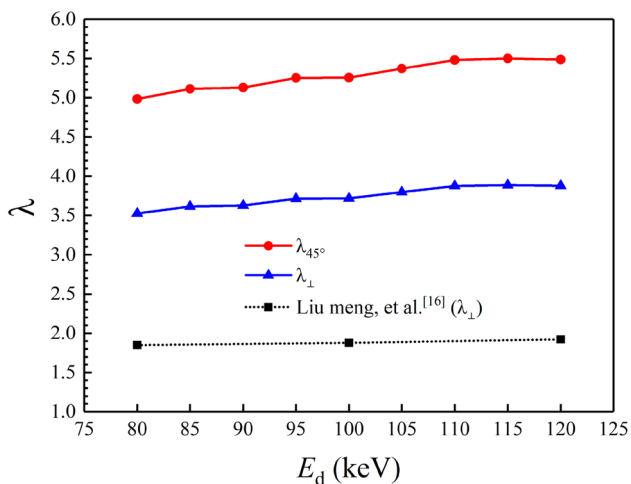
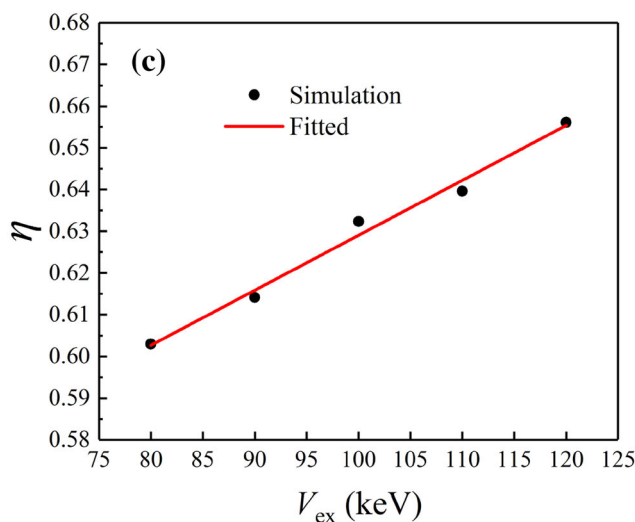
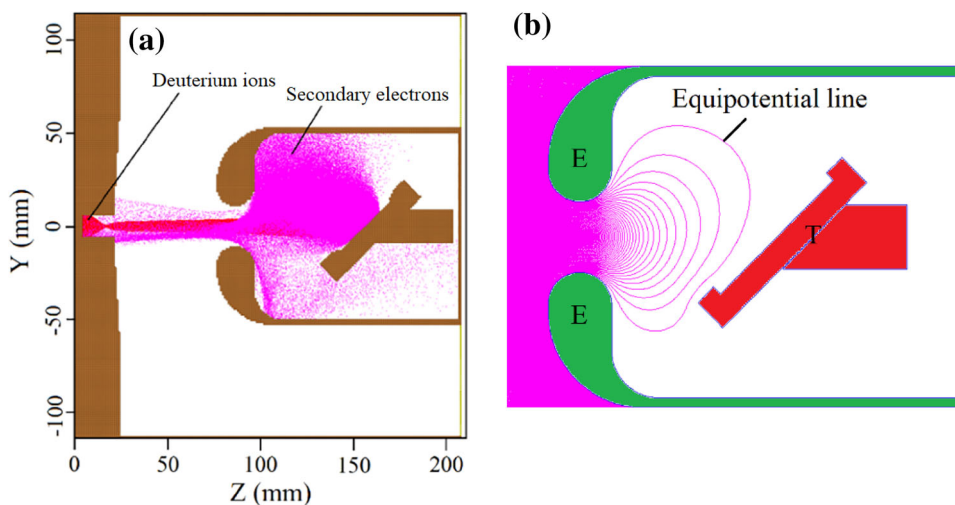


Fig. 8 Secondary electron emission coefficient (λ) for deuterium beam incident on molybdenum as a function of the deuterium energy (E_d)

beam (D_1^+ , D_2^+ , and D_3^+) is used in our experiment. The previous experimental results show that the coefficient (λ_{\perp}) for D_2^+ ions is about two times that of equal-energy D_1^+ ions [23]. According to our previous experimental results [24], the proportion of D_1^+ ions in the mixed deuterium ion beam (D_1^+ , D_2^+ , and D_3^+) is $< 10\%$ under the condition of low arc current (such as $I_{arc} < 1$ A) for the duoplasmatron ion source.

3 Conclusions

An experimental study of two methods for secondary electrons suppression in CDDNG was carried out. The methods are the electrostatic suppression and the magnetic suppression. Both methods can effectively suppress secondary electrons. By comparison, the designed electric field method is superior to the designed magnetic field method. Therefore, the electric field method will be applied

in our CDDNG. The resistance will be taken as 500 k Ω for a better suppression effect in a lower deuterium ion current.

The secondary electron emission coefficient for the mixed deuterium ions incident on molybdenum is estimated based on the experimental data of the electrostatic suppression. In the deuterium energy range of 80–120 keV, the estimated secondary electron emission coefficients are approximately 5–5.5 for mixed deuterium ion with glancing incidence of 45° and 3.5–3.9 for mixed deuterium ion with normal incidence. The above results may help to analyze the secondary electron problem in neutron tubes.

References

- H.Z. Bilheux, R. Mcgreevy, I.S. Anderson, *Neutron Imaging and Applications* (Springer, Boston, 2009), p. 67
- International Atomic Energy, Neutron Generators for Analytical Purposes, IAEA Radiation Technology Reports No. 1, IAEA, Vienna (2012)
- J.I.A. Fuquan, G.U. Deshan, C. Daowen et al., An neutron generator-based NIPGA system for on-site analysis. *Nucl. Sci. Tech.* **21**(1), 63–64 (2010). <https://doi.org/10.13538/j.1001-8042/nst.21.63-64>
- R. Ravisankar, P. Eswaran, N. Seshaderssan et al., Instrumental neutron activation analysis of beachrock samples of South East Coast of Tamilnadu, India. *Nucl. Sci. Tech.* **18**(4), 204–211 (2007). [https://doi.org/10.1016/S1001-8042\(07\)60047-5](https://doi.org/10.1016/S1001-8042(07)60047-5)
- Z.W. Huang, J.R. Wang, Z. Wei et al., Development of a compact DD neutron generator. *J. Instrum.* **13**(01), P01013 (2018). <https://doi.org/10.1088/1748-0221/13/01/P01013>
- A.G. Hill, W.W. Buechner, J.S. Clark et al., The emission of secondary electrons under high energy positive ion bombardment. *Phys. Rev.* **55**(5), 463 (1939). <https://doi.org/10.1103/PhysRev.55.463>
- I.H. Tan, M. Ueda, R.S. Dallaqua et al., Magnetic suppression of secondary electrons in plasma immersion ion implantation. *Appl. Phys. Lett.* **86**(2), 023509 (2005). <https://doi.org/10.1063/1.1852704>
- H.C. Bourne Jr., R.W. Cloud, J.G. Trump, Role of positive ions in high-voltage breakdown in vacuum. *J. Appl. Phys.* **26**(5), 596–599 (1955). <https://doi.org/10.1063/1.1722047>
- R. Adams, L. Bort, R. Zboray et al., Development and characterization of a D-D fast neutron generator for imaging applications. *Appl. Radiat. Isot.* **96**, 114–121 (2015). <https://doi.org/10.1016/j.apradiso.2014.11.017>
- M.A. Wasaye, H. Wang, P. He, An algorithm for Monte Carlo simulation of bremsstrahlung emission by electrons. *Nucl. Sci. Tech.* **28**(5), 65–73 (2017). <https://doi.org/10.1007/s41365-017-0218-7>
- J.E. Bouden, P.D. Lomer, J. Wood, A neutron tube with constant output (10¹⁰ n/sec) for activation analysis and reactor applications. *Nucl. Instrum. Methods.* **33**(2), 283–288 (1965). [https://doi.org/10.1016/0029-554X\(65\)90055-8](https://doi.org/10.1016/0029-554X(65)90055-8)
- S.G. Forbes, E.R. Graves, R.N. Little, Low voltage 14 MeV neutron source. *Rev. Sci. Instrum.* **24**(6), 424–427 (1953). <https://doi.org/10.1063/1.1770737>
- A.S. Tsybin, A.E. Shikanov, Neutron generation in small sealed accelerating tubes. *Russ. Phys. J.* **28**(8), 609–632 (1985). <https://doi.org/10.1007/BF00895162>
- I.J. Kim, H.D. Choi, Development of D–D neutron generator. *Nucl. Instrum. Meth. B* **241**(1–4), 917–920 (2005). <https://doi.org/10.1016/j.nimb.2005.07.170>
- C. Waltz, M. Ayllon, T. Becker et al., Beam-induced backstreaming electron suppression analysis for an accelerator type neutron generator designed for ⁴⁰Ar/³⁹Ar geochronology. *Appl. Radiat. Isot.* **125**, 124–128 (2017). <https://doi.org/10.1016/j.apradiso.2017.04.017>
- B. Goplen, L. Ludeking, D. Smith et al., User-configurable MAGIC for electromagnetic PIC calculations. *Comput. Phys. Commun.* **87**(1–2), 54–86 (1995)
- H. Nguyen, J. Mankowski, J.C. Dickens et al., Calculations of secondary electron yield of graphene coated copper for vacuum electronic applications. *AIP Adv.* **8**(1), 015325 (2018). <https://doi.org/10.1063/1.5019360>
- J.L. Wurtz, C.M. Tapp, Secondary electron emission from scandium, erbium, scandium deuteride, and erbium deuteride under deuteron bombardment. *J. Appl. Phys.* **43**(8), 3318–3324 (1972). <https://doi.org/10.1063/1.1661714>
- J.L. Ke, M. Liu, C.G. Zhou, Deuteron induced secondary electron emission from titanium deuteride surface. *Nucl. Instrum. Meth. B* **280**, 1–4 (2012). <https://doi.org/10.1016/j.nimb.2012.02.033>
- M. Liu, J.L. Ke, G. Huang et al., *Measurement of the secondary electrons emission efficiency from molybdenum induced deuteriums* (Nucl. Electron. Detect. Technol., Beijing, 2012). (in Chinese)
- R.A. Langley, J. Bohdansky, W. Eckstein et al., Data compendium for plasma-surface interactions. *Nucl. Fusion* **24**(S1), S9 (1984). <https://doi.org/10.1088/0029-5515/24/S1/001>
- S.B. Svensson, G. Holmen, A. Buren, Angular dependence of the ion-induced secondary-electron yield from solids. *Phys. Rev. B* **24**(7), 3749 (1981). <https://doi.org/10.1103/PhysRevB.24.3749>
- G.W. McClure, High-voltage glow discharges in D₂ gas. I. Diagnostic measurements. *Phys. Rev.* **124**(4), 969 (1961). <https://doi.org/10.1103/PhysRev.124.969>
- B.H. Sun, Q. Chen, Characteristics of intense beam for a duoplasmatron source. *Nucl. Tech.* **14**(12), 731–737 (1991). (in Chinese)